Geometric Analysis of Diffusion Pathways in Glassy and Melt Atactic Polypropylene

Michael L. Greenfield and Doros N. Theodorou*

Department of Chemical Engineering, University of California, Berkeley, Berkeley, California 94720

Received April 14, 1993®

ABSTRACT: Glassy and melt atactic polypropylene microstructures obtained via energy minimization and Monte Carlo simulation are subjected to geometric analysis (Delaunay tessellation followed by volume and connectivity analysis) in order to determine the clusters of sites where a hard sphere penetrant of radius 0–2.5 Å can reside. A variety of cluster volumes are found for each penetrant radius, and typical clusters are visualized for methane, helium, and two hypothetical penetrants of smaller radius. Peaks are observed in the distribution of cluster volumes, representing characteristic hole sizes induced by local packing. The cluster root-mean-square radius of gyration and average accessible volume decrease monotonically for penetrants larger than helium. A hypothetical penetrant of radius ca. 0.9 Å can percolate the polymer structure, whereas the same size penetrant is trapped in a random close-packed (rcp) configuration of spheres with diameter commensurate with the polymer segments. Clusters accessible to small penetrants are used to isolate probable pathways for diffusion, and the connectivity of the network of clusters is quantified. Visualization of thermal fluctuations of clusters shows two kinds of mobility. In the melt, polymer fluctuations induce rapid cluster rearrangement. In the glass, clusters retain their identity, while thermal fluctuations infrequently open and close diffusion pathways between them. A methodology for applying this work to full energy-based calculations of diffusivity in the glass using multidimensional transition-state theory is introduced.

Many products and processes rely on the diffusion of small molecules through a polymer film. In gas permeation, differing diffusion rates are used to separate gas mixtures. Other applications, such as food packaging and beverage containers, require a diffusive barrier. To design these systems one must measure, correlate, or predict the diffusivity of several penetrants (gases or liquids) in various polymers.

Phenomenological models invoke a coarse-grained physical picture to correlate diffusivity with molecular parameters. The free volume approaches[1–4] relate diffusive penetrant motion to the redistribution of space not occupied by polymer chains. Other models treat the diffusive process as a sequence of activated hopping motions,[5–9] for which a specific molecular mechanism is assumed and the resulting transition energetics is calculated. The dual mode diffusion model presupposes two types of sorption sites, with the jump rate between two adjacent sites depending upon the identity of both sites.[10] In general, phenomenological models have correlated results successfully, but do not enable an a priori prediction of the diffusivity for a particular penetrant–polymer system. Such a prediction requires accounting for the detailed molecular interactions that underlie the macroscopic behavior. Calculations of this type have been performed in the past, as discussed below. However, improvements can still be made. The present paper discusses a geometrical analysis conducted en route to predicting the diffusivity of a dilute penetrant gas in a glassy polymer.

Prediction of the diffusivity from "first principles" requires a detailed representation of the configuration of and molecular interactions amongst the atoms of the polymer and the penetrant. Jagodic et al.[11] were the first to attempt a computer calculation of the diffusion coefficient from the potential energy along a diffusion path. Due to the limited computational resources available to them in the early 1970s, they were unable to generate a realistic polymer structure or to attain correct potential energy barriers. Recently, molecular dynamics (MD) studies of gas diffusion have been performed in the melt[12–21] and in the glass.[22] Although predicting the diffusivity in some melts may be feasible using MD,[15,20,21] predicting the diffusivity in the glass is not, because the characteristic diffusion time greatly exceeds the time that can be simulated with available computational means. This necessitates more coarse-grained approaches. However, MD simulations in the glass have elucidated important mechanistic aspects of diffusion: fluctuations in the configuration of the polymer infrequently open a pathway between the location of the penetrant and another sorption site. This allows the penetrant to move or hop between sites, as shown pictorially by Takeuchi.[22] The frequency of these fluctuations can be estimated to be on the order of ns^{-1} in the melt from plots of Müller-Plathe[14] or Sok et al.[21]

Suter and co-workers have approximated the true dynamics and calculated penetrant hopping rates (and ultimately diffusivities) using transition-state theory (TST). Arizzi[23] considered penetrant motion between tetrahedral interstices of a static model glassy polymer. Gusev et al.[24,25] considered penetrant diffusion through both static polymers and model polymers with atoms bound harmonically to their equilibrium positions, about which they execute independent vibrations. The amplitude of the position fluctuations is a parameter extracted from short-time MD simulations. In static glassy polycarbonate and static melt polyisobutylene the predicted diffusivity of helium was of the correct order of magnitude. Prediction was unsuccessful for hydrogen and larger penetrants because of the imposed polymer rigidity; the predicted diffusivity in the static structures was orders of magnitude too small. In fluctuating glassy polycarbonate and fluctuating melt polyisobutylene, the predicted diffusivities of light gases were of the correct order of magnitude.

We wish to investigate dilute penetrant diffusive motion within a glassy polymer in a more detailed manner. Rather

* To whom correspondence should be addressed.
® Abstract published in *Advance ACS Abstracts*, September 1, 1993.

0024-9297/93/2226-5461$04.00/0

than consider diffusion through a static model polymer or a polymer with Gaussian fluctuations in atomic positions, we plan to use multidimensional TST to incorporate the polymer degrees of freedom explicitly into the calculation of rate constants for penetrant hopping. We feel that such an approach is necessary for a realistic treatment of diffusive hops of large penetrants, which may occur only as a consequence of significant conformational rearrangements of the surrounding polymer. Such a coupling between penetrant diffusion and torsional motions in the melt was observed by Pant and Boyd[20] and by Takeuchi and Okazaki,[26] who reported a decrease (increase) in the diffusivity when torsional barriers were raised (lowered) during an MD simulation.

One difficulty of such a multidimensional TST calculation is the multitude of local potential energy minima (sorption states) of the penetrant–polymer system. Physical intuition suggests and MD trajectories have confirmed[22] that these local minima are not evenly dispersed throughout the configuration space of the penetrant–polymer system. We expect the penetrant coordinates of local minima to cluster together within relatively open spaces in the glassy matrix, forming "macrostates" of local minima. Within a macrostate, the local minima are separated by energy barriers small relative to the thermal energy kT. Transitions in configuration space between macrostates should be much slower than motions within a macrostate. Physically, the penetrant must "squeeze" open a path between chains, and motion involving normal modes of the chains should be crucial to the transition. These rare transitions are the controlling step of diffusive motion and are the barrier crossings to which we will apply transition-state theory.

The ease of searching for stationary points (local minima and transition states) of a multidimensional function depends on the initial estimates available. Generation of amorphous polymer configurations is possible using the actual potential energy.[27-29] Such approaches require a first approximation for the structure, such as a set of RIS chains. Likewise, addressing the multidimensional TST problem requires an appropriate initial guess for the diffusion paths. Our approach is to generate polymer configurations using the methods referenced above, and then to approximate the penetrant–polymer potential energy function as a hard sphere interaction. This reduces the identification of sorption sites and diffusion pathways to a geometric problem—where can a hard sphere penetrant fit within a set of hard polymer atoms?

The molecular geometry of penetrant–polymer systems has been addressed previously. The aim of past geometric work was to characterize the volume within the polymer where a penetrant could reside. Shah et al.[30] used a Monte Carlo integration approach in which they selected points randomly within their model polymer structures and determined the largest diameter of a sphere that could be inserted at each point. Arizzi et al.[31] divided their static structures of polycarbonate and atactic polypropylene into tetrahedral interstices using Delaunay tessellation and approximated the unoccupied volume in each interstice. They reported the size distributions of tetrahedral vacancies and of clusters of connected vacancies. Trohalaki et al.[32] proposed a model in which unoccupied voids in a polymer melt are treated as independent sites; they predicted that the probability of observing a void of volume V decreases exponentially with increasing V. Rigby and Roe[33] analyzed the distribution of Voronoi polyhedra and cavity volumes encountered during an MD simulation of alkanes and observed slow fluctuations in the cavity locations and polydispersity in the cavity sizes. Weiss et al.[34] have developed a formalism to describe sorption data in polymers using a distribution of "unrelaxed density fluctuations", where the size of the fluctuation is analogous to the size of an accessible site. Kirchheim[35] proposed a model for sorption behavior using a Gaussian distribution of site volumes and energies. Gusev and Suter[36] used geometric considerations in conjunction with energy calculations in order to partition a static polymer structure into sorption sites. The sorption isotherm of methane in polycarbonate was calculated on the basis of these geometric divisions and agreed reasonably with experiment.

We are using geometric analysis as a prelude to the more elaborate multidimensional TST calculations discussed above. The three-dimensional closed domains accessible to a hard sphere penetrant in pure polymer structures provide a first approximation to the penetrant position macrostates where the penetrant would spend most of its time. Regions between two macrostates accessible to a hypothetical hard sphere penetrant of smaller diameter than the one of interest approximate pathways between the macrostates. Small, hypothetical hard sphere penetrants probe regions of the polymer structure inaccessible to hard spheres the size of a real penetrant; these regions are of interest because real penetrants feel a soft potential from the polymer matrix, and the matrix responds to the presence of the penetrant, allowing the real penetrant to explore more of the structure than can a hard sphere.

In this paper we describe our implementation of a geometric analysis of glassy polymer structure. In particular, we extend the work of Arizzi et al.[31] by determining both averages and underlying distributions of cluster volume shapes and sizes, as probed by a variety of penetrants in thermally fluctuating configurations of pure glassy and melt atactic polypropylene. The multichain configurations representing the glass and melt are obtained from detailed simulations of the pure polymer. While the simulations employ detailed atomistic potentials, a hard sphere representation is used in the geometric analysis for both the polymer interaction sites and the penetrant probe. The simulations were conducted in the absence of penetrant. Thus pure polymer structures are analyzed in order to determine the regions where a hard sphere penetrant can fit without disturbing the polymer. Such locations are the most likely sites where sorption may occur, and paths between these sites represent first approximations of the paths taken by a penetrant during diffusive hopping events.

Model and Methods

The goal of our geometric analysis is to determine where (in the polymer) a penetrant center may reside, how the shapes of these accessible regions are distributed and connected, and how the accessible regions change with penetrant size. The polymer configurations analyzed consist of three 50-unit (100 skeletal bond, molecular weight 2120) chains of equilibrium atactic polypropylene in an orthorhombic cell with periodic boundary conditions and edge lengths of approximately 23 Å. Penetrant radii from 0 to 2.5 Å were considered. In order to discern the fine structure of the accessible regions, we conceptually subdivide each microstructure into many small pieces, analyze each piece, and then fuse the pieces together. We use a modification of Arizzi's procedure:[31] tessellation of space into Delaunay tetrahedra, calculation of the accessible volume inside each tetrahedron, and fusion of adjacent accessible tetrahedra into clusters.

Generation of Polymer Structures. Starting configurations for the glassy polymer were generated as local minima in the potential energy hypersurface by molecular mechanics, using the technique of blowing up the atomic radii.[27] Fluctuations around

Table I

penetrant	r_p (Å)[a]	ref	penetrant	r_p (Å)[a]	ref
zero size	0		helium	1.28	39
(hypothetical)	0.25		neon	1.53	39
(hypothetical)	0.50		(hypothetical)	1.74	
(hypothetical)	0.63		argon	1.91	39
(hypothetical)	0.75		methane	2.09	40
(hypothetical)	0.90		xenon	2.30	41
(hypothetical)	1.00		ethane	2.50	41
(hypothetical)	1.10				

[a] The van der Waals radius, calculated as $r_p = (\sigma/2)2^{1/6}$, where σ is the length parameter of the Lennard–Jones potential.

a local glassy minimum were explored with constant temperature (233 K) and pressure (1 atm) Monte Carlo (NPTMC) using concerted rotations.[28,37] The degrees of freedom and parameters of the polymer structure model are described elsewhere.[28] Fourteen initial structures were generated, and twelve were tracked for five million attempted NPTMC moves each. One of the structures was tracked for 20 million moves, and another for 30 million moves. Other system sizes were also investigated: two systems with two 50-unit chains and one system with six 50-unit chains. A three-chain system was also investigated at 400 K, at which temperature atactic polypropylene is a melt. In each NPTMC run with a three-chain system, the initial two million moves were used for "equilibration"; configurations from later in the simulation were used to calculate geometric properties. The number of "equilibration" moves varied according to the system size. The minimization scheme results in independent, quenched local minima. Concerted rotation moves are an attempt to sample the thermal fluctuations of the glassy polymer in a Monte Carlo fashion. NPTMC explores the region of configuration space in the vicinity of a local minimum, configurations near the minimum being visited according to Boltzmann weighting. Thus, averages for each local minimum are "annealed", and the average over the glassy system is calculated by arithmetic (spatial) averaging over the different local minima. The annealed average $\bar{A}_j$ of a property A about local minimum j is calculated by averaging over all fluctuations,

$$\bar{A}_j = \sum_{i=1}^{N_j} (\text{weight})_i A_{ij} \Big/ \sum_{i=1}^{N_j} (\text{weight})_i \qquad (1)$$

where N_j is the number of configurations about local minimum j used in the geometric analysis and A_{ij} is the value of A in configuration i. "(weight)$_i$" signifies either a number-weighted or a volume-weighted average over the accessible volume clusters of configuration i; the weighting chosen is indicated in the text describing the property of interest. The arithmetic average $\langle A \rangle$ over $N = 14$ independent local minima is calculated as

$$\langle A \rangle = \frac{1}{N} \sum_{j=1}^{N} \bar{A}_j \qquad (2)$$

Tessellation of Space. Given a collection of points in space, Delaunay tessellation partitions them into irregular tetrahedra such that the circumsphere of each tetrahedron is devoid of points except for those lying on the vertices. In our case, the atomic centers of the polymer chains form the collection of points. A Delaunay tetrahedron corresponds to four neighbors surrounding a small interstitial hole in the polymer. The algorithm of Tanemura[38] was used for the Delaunay tessellation and is described elsewhere.[31,38]

Volume Calculation. Fifteen different penetrant radii were considered, some corresponding to realistic gaseous penetrants and some to smaller hypothetical penetrants. The smallest was a penetrant with zero radius; the largest corresponded to a spherical approximation for ethane. The van der Waals radius (equal to half the center-to-center distance at the minimum of the Lennard–Jones potential for two interaction sites of the same kind) was used as the hard sphere radius for each penetrant and each site in the polymer. van der Waals radii for the penetrants are listed in Table I.

We obtain the exact occupied volume inside each tetrahedron analytically using a method which calculates the volume of an arbitrary number of overlapping spheres intersected by planes.[42] First, we determine which atoms intersect the tetrahedron's circumsphere. Next, we calculate the volume that this set of atoms occupies inside the tetrahedron. Any volume in the tetrahedron not occupied by atoms was termed by Arizzi et al.[31] "unoccupied volume", and the sum of the unoccupied volume over all tetrahedra divided by the total system volume equals the unoccupied volume fraction ϕ^{unocc}. The volume accessible to a penetrant of radius r_p is found by first augmenting the van der Waals radius of each atom in the polymer by r_p and then calculating the volume that remains unoccupied by the augmented polymer atoms, using the procedure above. This latter volume we term the accessible volume $V^{\text{acc}}(r_p)$. It is the volume within the tetrahedra accessible to the center of a spherical penetrant of radius r_p and is a function of r_p. By these definitions, the unoccupied volume coincides with the accessible volume for a zero radius penetrant. Both unoccupied volume and accessible volume are defined pictorially in Figure 1.

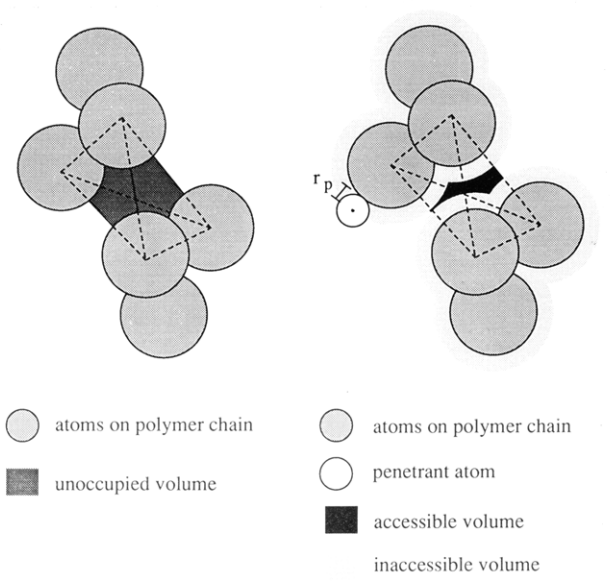

Figure 1. Unoccupied and accessible volume in a sample tetrahedron. The unoccupied volume is the volume not occupied by atoms of the polymer. The accessible volume is the volume accessible to the center of a penetrant of radius r_p and can be found by "rolling" the penetrant on the inner surface of the unoccupied volume.

Cluster Formation. Each Delaunay tetrahedron shares its faces with four other tetrahedra. Some of these faces are "sufficiently open" to allow movement of a hard sphere penetrant directly from one tetrahedron to another.[31] When this happens, we say that the two tetrahedra are directly connected for the penetrant radius under examination. Tetrahedra with common directly connected neighbors are connected indirectly and form clusters of accessible volume. Such clusters may be small (a large penetrant in a large void or a small penetrant in a small void) or extended pathway structures (for small penetrants). The list of tetrahedra in a cluster is generated using a connectivity matrix algorithm.[43] Note that joining mutually accessible tetrahedra into clusters "integrates" over (and loses memory of) the artificial tetrahedral tessellation. The microstructure could equally well have been divided into many small cubes, with clusters being the union of connected accessible cubes. The advantage of Delaunay tessellation is the physical interpretation of tetrahedra as interstitial holes.

Cluster Volume Analysis. Since the center of a hard sphere penetrant can visit all locations within a cluster (by definition), the geometric properties of clusters provide an approximate description of sorption sites. We define two cluster size distributions to characterize the various cluster volumes observed during the simulations. The number fraction of clusters with a volume V to $V + dV$ accessible to a penetrant of radius r_p is termed $n(V;r_p)dV$. The volume fraction of clusters with a volume V to $V + dV$ accessible to a penetrant of radius r_p is termed $\rho(V;r_p)dV$. Both distributions are normalized to unity, and they

are related by

$$\rho(V;r_p) = \frac{n(V;r_p)V}{\int_0^\infty n(V;r_p)V\,dV} \tag{3}$$

$\rho(V;r_p)$ is also called the accessible volume probability density distribution and is an average of the distributions found around each local potential energy minimum. For all configurations that sample fluctuations around a local potential energy minimum j, $\rho_j(V;r_p)$ was calculated by averaging over the clusters accessible to a particular penetrant radius (compare eq 1)

$$\rho_j(V;r_p) = \frac{1}{\sum_i V_{ij}} \sum_i V_{ij}\delta(V - V_{ij}) \tag{4}$$

which we approximate as

$$\rho_j(V;r_p) = \frac{1}{\sum_i V_{ij}} \sum_i V_{ij} \frac{1}{\Delta V}\int_V^{V+\Delta V} \delta(V - V_{ij})\,dV \tag{5}$$

where V_{ij} equals the accessible volume of cluster i within a configuration in the vicinity of local minimum j and ΔV equals 5.64 Å^3. The integral of the δ function equals unity if V_{ij} is in the range V to $V + \Delta V$, and zero otherwise. Configurations around each j are Boltzmann-weighted by virtue of the NPTMC algorithm used for their generation. The total accessible volume probability density distribution $\rho(V;r_p)$ is an arithmetic average over the $N = 14$ "local minimum" probability distributions ρ_j, following eq 2. The number fraction distribution $n(V;r_p)$ is calculated in a similar manner.

The accessible volume fraction ϕ^{acc} equals the total volume of clusters per unit volume of polymer and is a function of penetrant radius. Its average is related to the first moment of the number weighted cluster volume probability density distribution,

$$\langle\phi^{acc}\rangle = \frac{1}{N}\sum_j \overline{\phi_j^{acc}} = \rho_{CL}\int_0^\infty n(V)V\,dV \tag{6}$$

where ρ_{CL} equals the average number of clusters per unit volume. The accessible volume fraction is related to sorption. The expression for the Henry's constant of a spherical gas in a rigid polymer matrix[36]

$$K_H = \frac{1}{kTV}\sum_{sites}\int_{site} \exp(-\mathcal{V}(x,y,z)/kT)\,dx\,dy\,dz \tag{7}$$

simplifies for hard spheres to

$$K_H = \frac{1}{kT}\langle\phi^{acc}\rangle \tag{8}$$

since the Boltzmann factor equals unity for accessible sites and zero otherwise. Thus, the average accessible volume fraction would govern low occupancy sorption in a rigid, hard sphere system.

Cluster Shape Analysis. Each cluster's size and shape were quantified using a radius of gyration matrix[31,44]

$$\mathbf{S} = \begin{pmatrix} \overline{xx} & \overline{xy} & \overline{xz} \\ \overline{yx} & \overline{yy} & \overline{yz} \\ \overline{zx} & \overline{zy} & \overline{zz} \end{pmatrix} \tag{9}$$

where

$$\overline{xx} = \sum_{i=1}^{N_T} w_i x_i x_i \tag{10}$$

$$\overline{xy} = \sum_{i=1}^{N_T} w_i x_i y_i, \text{ etc.}$$

The sum is over the N_T tetrahedra in the cluster, (x_i,y_i,z_i) is the centroid of tetrahedron i relative to the volume-weighted centroid of the cluster, and w_i is the accessible volume of tetrahedron i divided by the accessible volume of the cluster. This differs from Arizzi's definitions in that we calculate $\mathbf{S}$ using the centroids of tetrahedra weighted by their accessible volume, rather than as an unweighted average over the atoms which belong to the cluster. The eigenvalues of $\mathbf{S}$ are determined and sorted such that

$$\overline{X^2} \geq \overline{Y^2} \geq \overline{Z^2} \tag{11}$$

The squared radius of gyration, s_{ij}^2, and dimensionless asphericity, $(b/s^2)_{ij}$, of cluster i within a configuration in the vicinity of local minimum j are found from the eigenvalues:[44]

$$s_{ij}^2 = \overline{X^2} + \overline{Y^2} + \overline{X^2} \tag{12}$$

$$(b/s^2)_{ij} = \frac{\overline{X^2} - \frac{1}{2}(\overline{Y^2} + \overline{Z^2})}{\overline{X^2} + \overline{Y^2} + \overline{Z^2}} \tag{13}$$

These eigenvalues reflect the squared lengths of the three different principal axes of the cluster. The averages over fluctuations about each local minimum were calculated with volume weighting in the spirit of eq 1:

$$\overline{s_j^2} = \frac{\sum_{i=1}^{N_{cj}} V_{ij}\, s_{ij}^2}{\sum_{i=1}^{N_{cj}} V_{ij}} \tag{14}$$

where N_{cj} is the total number of clusters encountered in configurations sampling fluctuations around local minimum j. The average cluster radius of gyration and asphericity were calculated as arithmetic averages, following eq 2. Average asphericity is calculated identically by replacing s^2 by b/s^2 in eq 14 and averaging with eq 2.

Error Analysis. Error estimates on shape parameters, volume distributions, and volume fractions were calculated assuming that all configurations of a cluster encountered within an NPTMC simulation around the same local minimum were strongly correlated with one another, by virtue of the physically "locked-in" nature of a glass. All different snapshots of the same cluster obtained in the course of an NPTMC run were treated as a single sample (one averaged point) in the error analysis. Error bars reflect the standard deviation of the mean from our $N = 14$ independent local minima. This is a conservative estimate of the random errors, in that we assumed perfect correlation among fluctuations about each local minimum.

Connectivity Analysis. Clusters of accessible volume provide a geometric approximation to the sorption states. While a hard sphere penetrant in a rigid polymer matrix would be confined to the sorption states, a soft core penetrant infrequently accesses pathways between states as it diffuses through the polymer. The jump motion observed by Takeuchi[22] relied on a slight rearrangement of polymer chains to open a channel between two sites. A geometric approach of searching for locations where such fluctuations are likely is to analyze the volume accessible to a small, hypothetical penetrant which can percolate the model box of polymer. We propose that the clusters accessible to such a small, hypothetical penetrant provide a first approximation to the pathways traversed by a real penetrant interacting with the polymer. In the next paragraphs we discuss an algorithm for mapping clusters accessible to the penetrant of interest onto the volume accessible to a small hypothetical penetrant, thereby determining the connectivity among clusters.

In each particular polymer configuration, for a sufficiently small penetrant radius there exists an accessible cluster which spans the periodic model system and intersects images of itself. Such a cluster is termed a percolating cluster of accessible volume.[45] Our scheme is to partition the percolating cluster into a set of distinct regions: some are accessible to the original penetrant of interest; others are accessible only to smaller penetrants. The latter regions identify passages between the

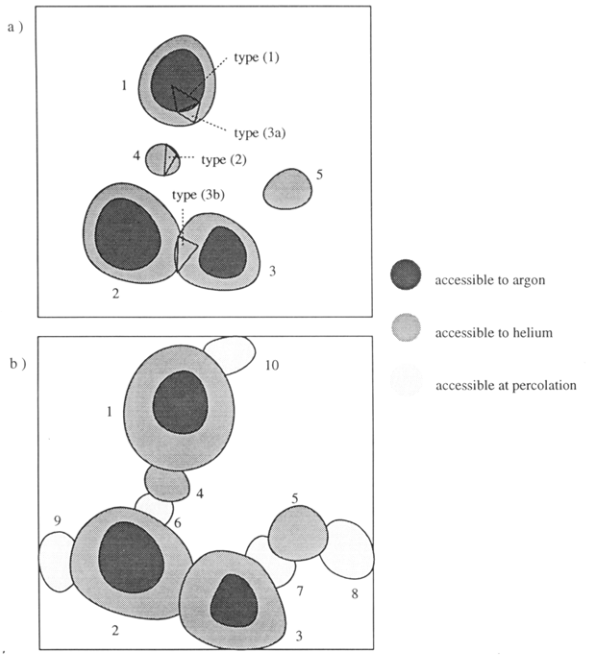

Figure 2. 2D schematic of the connectivity algorithm. (a) Clusters 1–3 are accessible to the original penetrant (e.g. argon), and clusters 1–5 are accessible to a smaller penetrant (e.g. helium). Different types of tetrahedra are discussed in the text. (b) Partitioning of the percolating cluster into clusters. Clusters 6–10 are not accessible to argon and helium but are accessible to smaller penetrants.

disjoint clusters accessible to the penetrant of interest. This partitioning, displayed schematically in Figure 2b, is performed on the level of the Delaunay tetrahedra that comprise the percolating cluster by labeling each tetrahedron with the identity of the disjoint cluster to which it belongs when first becoming accessible. The connectivity among clusters is then determined from the connectivity among tetrahedra in the infinite cluster.

The first step is to identify the clusters accessible to the penetrant of interest, indicated by dark shading in Figure 2. Each cluster consists of many tetrahedra, and these tetrahedra are labeled according to the number of the cluster to which they belong (1–3), as shown in Figure 2a for cluster 1. The clusters accessible to the next smaller penetrant are then considered, shown by the medium shading in Figure 2a. The tetrahedra in each of the clusters accessible to this smaller penetrant are divided into three categories: (1) tetrahedra accessible to the larger penetrant, (2) tetrahedra inaccessible to the larger penetrant and isolated from any cluster accessible to the larger penetrant, and (3) tetrahedra inaccessible to the larger penetrant but connected to a cluster of tetrahedra accessible to the larger penetrant. The identity of type 1 tetrahedra is already known from previous steps of the connectivity algorithm. Type 2 tetrahedra signal the emergence of a new cluster that was inaccessible to the original penetrant; the number of disjoint clusters is incremented by one, and the tetrahedra in this cluster are assigned this new cluster number (4, 5, ...), as shown for cluster 4 in Figure 2a. Type 3 tetrahedra are subdivided further into (3a) sets of tetrahedra connected to only one preexisting cluster and (3b) sets of tetrahedra connected to two or more preexisting clusters. Type 3a tetrahedra are labeled with the number of the cluster to which they are connected, as shown for cluster 1 in Figure 2a. Type 3b tetrahedra are considered sequentially. Each tetrahedron is assigned the cluster number of a neighbor tetrahedron with which it is directly connected. If none of the neighbors of a tetrahedron have been assigned a label, we refrain from labeling the tetrahedron in the current pass. We loop repeatedly over all type 3b tetrahedra until all have been labeled. For example, the type 3b tetrahedra in Figure 2a would be labeled either "2" or "3" after all passes were completed. Thus, around each prexisting sorption state, the newly created "shell" of tetrahedra accessible to the smaller penetrant is labeled one layer at a time.

After all accessible tetrahedra have been labeled for a particular penetrant, we consider the next smaller penetrant radius and proceed exactly as described above. The process is repeated for smaller and smaller penetrant radii until some lower limit of the penetrant radius is reached; in this work, the lower limit equals the percolation threshold of the configuration under examination. At this point, each accessible tetrahedron in the percolating cluster is labeled with its cluster number, and the set of clusters form a network, as in Figure 2b. A direct connectivity matrix for the clusters is created, in which element ij equals unity if clusters i and j are directly connected, and zero otherwise. Direct connectedness is determined by comparing the cluster number (the label) of each accessible tetrahedron with that of its direct tetrahedral neighbors. For example, in Figure 2b the clusters numbered "1" and "2" are indirectly connected, while clusters numbered "1" and "4" are directly connected. Finally, a variation of the connectivity algorithm of ref 43 is used to determine the indirect connectivity among those clusters accessible to the penetrant of interest, based on the information contained in the direct connectivity matrix. In Figure 2b, cluster "1" is connected to two other clusters ("2" and an image of "3") accessible to the penetrant of interest, while cluster "2" is connected to three clusters ("1", "3", and an image of "3") accessible to the penetrant of interest. By considering connectivity in the entire collection of structures, we calculate the volume-weighted average number of connected neighbors, $p(n)$. In the vicinity of a minimum energy configuration j,

$$p_j(n) = \sum_{i=1}^{N_{cj}} V_{ij}\delta_{n_{ij}n} \Big/ \sum_{i=1}^{N_{cj}} V_{ij} \qquad (15)$$

where n_{ij} equals the number of paths emanating from cluster i encountered in a configuration that lies in the vicinity of local minimum j, and $\delta_{n_{ij}n}$ equals unity if $n_{ij} = n$ and zero otherwise (Kronecker δ). Arithmetic averaging of $p_j(n)$ over different glassy minima j in order to obtain $p(n)$ is performed as in eq 2.

Results and Discussion

The geometric properties of accessible clusters depend upon the penetrant size r_p. Within the set of clusters accessible to a particular penetrant, there is a distribution of sizes and shapes. For large penetrants, the accessible regions form small voids that are well separated from one another. For smaller penetrants, paths link clusters into larger networks. Figure 3 depicts the volume accessible to four penetrants in one particular configuration of glassy atactic polypropylene obtained in the course of an NPTMC simulation. For a spherical penetrant approximating methane (radius r_p = 2.09 Å), this configuration contains three clusters, well separated from one another. For a smaller penetrant the size of helium (r_p = 1.28 Å), new regions become accessible to the penetrant center. Two observations can be made. First, accessible regions "fuse together" into larger clusters (e.g., the red and blue methane-accessible clusters fuse into one helium cluster). Second, new clusters emerge in regions which were previously inaccessible (e.g., the gray and yellow clusters in the helium picture). At an even smaller hypothetical penetrant radius of r_p = 1.1 Å, more pathways emerge and connect the larger clusters. For a hypothetical penetrant radius of 0.9 Å, an infinite cluster appears (in red) which entirely traverses (or percolates) the periodic box of polymer. This penetrant size is typical of the onset of percolation, as will be discussed later.

Cluster Volume Results. The average size of accessible clusters varies with the penetrant radius. The volume-weighted distribution of accessible cluster volumes $\rho(V;r_p)$ is plotted in Figure 4 for helium, neon, argon, and methane. In general, the probability that an accessible region belongs to a cluster of size between V and $V + dV$ decreases with increasing cluster volume V. Peaks in the distribution, such as those indicated with an overbar in

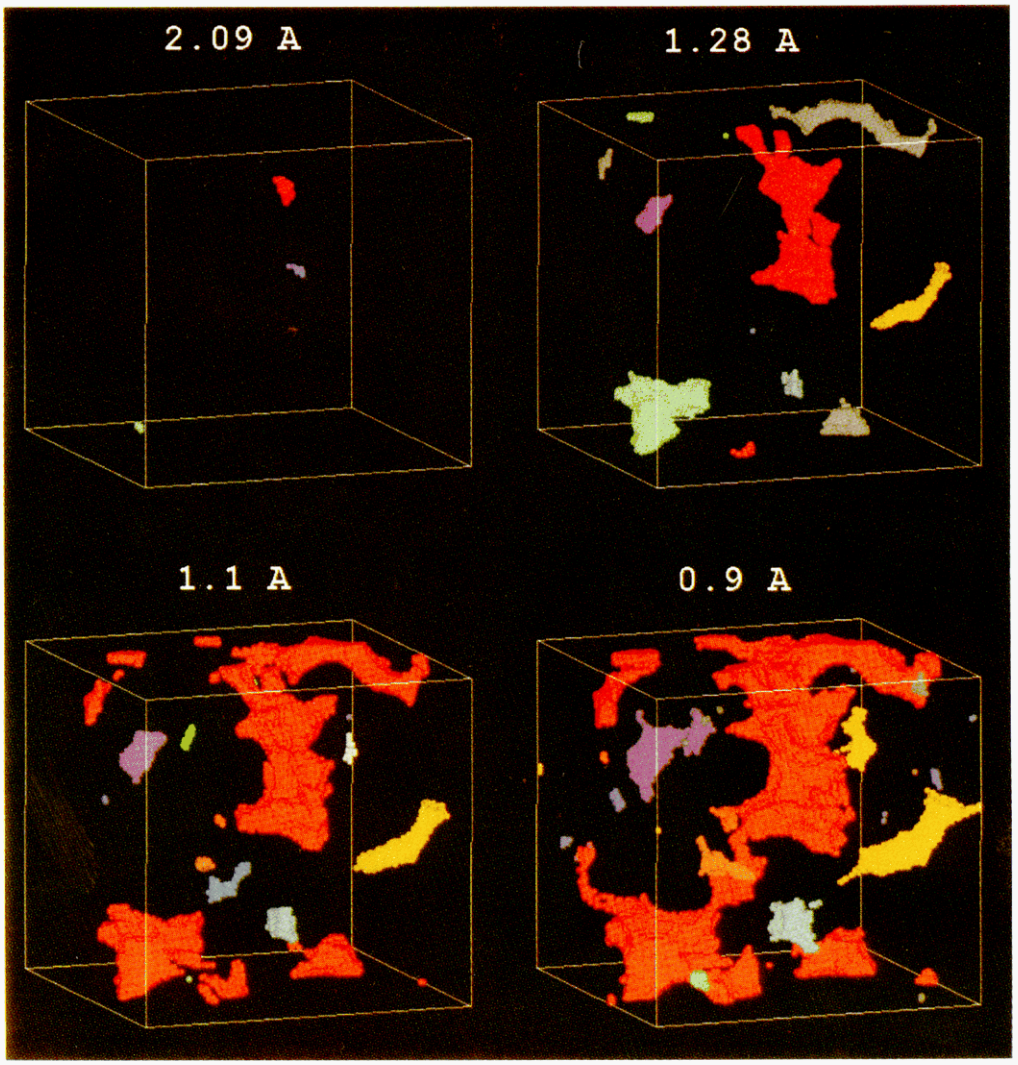

Figure 3. Clusters accessible to (a) methane (r_p = 2.09 Å), (b) helium (r_p = 1.28 Å), (c) a hypothetical penetrant of van der Waals radius r_p = 1.1 Å, and (d) a hypothetical penetrant of van der Waals radius r_p = 0.9 Å. Different colors indicate different clusters; wrapping over the box edge is due to periodic boundary conditions. The box edge is approximately 23 Å. As the penetrant radius decreases, accessible clusters grow and fuse together. Percolation is observed for the red cluster accessible to the penetrant of size r_p = 0.9 Å.

Figure 4, suggest that clusters of a particular size may be more probable than either slightly larger or smaller ones (within the error of the analysis). This is especially evident in the helium distribution. We propose that these cluster sizes are characteristic of the local packing of atactic polypropylene chains. Local packing depends on the chemical constitution and architecture of the polymer; the accessible cluster volume probability density for the same penetrants in other polymers would differ from that shown here for atactic polypropylene. Similar characteristic sizes have been observed by Jean and co-workers[46] in their measurements of free volume holes in an epoxy polymer using positron annihilation lifetime spectroscopy, in which the lifetime of a spin-aligned positron–electron pair, o-positronium (o-Ps), depends on the local electronic structure and thus on the size and distribution of unoccupied volume. The large error bars seen in the distributions for large cluster volumes are inescapable. More small clusters than large clusters are present in any instantaneous configuration of the fluctuating polymer, and the sampling of large clusters is correspondingly worse.

The characteristic cluster sizes seen in Figure 4 for neon, argon, and methane each correspond to the same "holes" among the chains and differ in volume mainly due to the different penetrant radii. A simple model explains this result. Consider a hole with unoccupied volume V as sampled by different sized penetrants. For spherelike holes, the volume is related to the cube of some characteristic length scale R,

$$V = kR^3 \tag{16}$$

where k is a constant (for a sphere $k = (4/3)\pi$ with R the sphere radius). The accessible volume should have a similar shape, but with a characteristic length decreased by the penetrant radius:

$$V^{acc} = k(R - r_p)^3 \tag{17}$$

Solving eq 16 for the characteristic length, substituting into (17), and taking the cube root result in

$$(V^{acc})^{1/3} \approx V^{1/3} - k^{1/3} r_p \tag{18}$$

In Figure 5 we plot as a function of penetrant radius the value of $(V^{acc})^{1/3}$ corresponding to the peak of the $\rho(V;r_p)$ distribution indicated with an overbar in Figure 4. The linearity seen for penetrants larger than helium suggests that these penetrants all probe the same "holes" of unoccupied volume V. Penetrants of smaller size sense more of the fine structure of the polymer matrix. For such penetrants, "fingers" of accessible volume extend

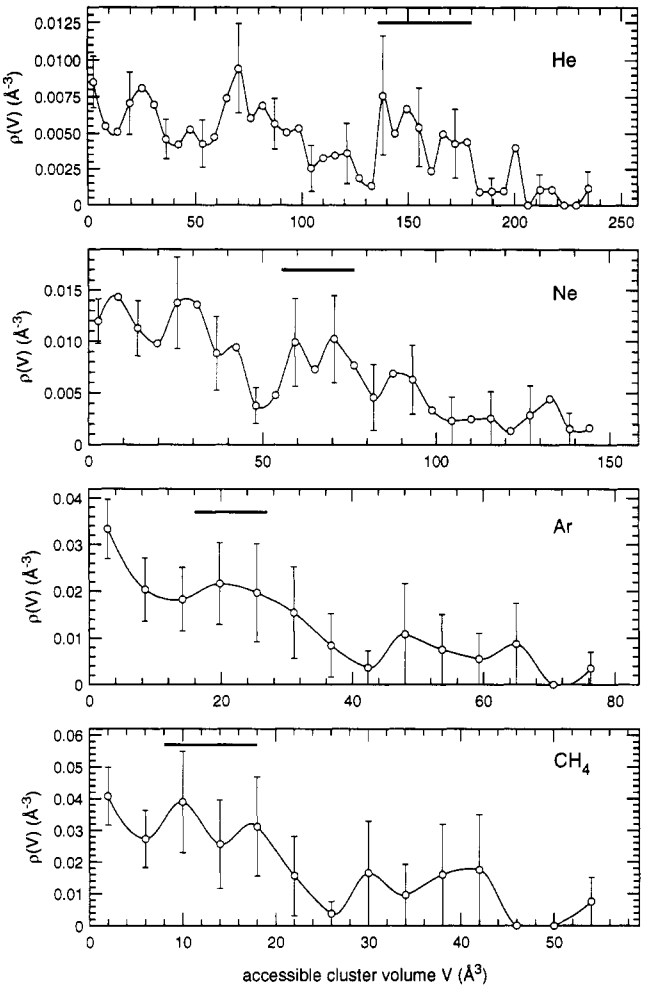

Figure 4. Probability density $\rho(V;r_p)$ that an accessible point lies in a cluster of volume V for (a) helium, (b) neon, (c) argon, and (d) methane. Error bars depict the standard deviation of the mean from fluctuations about 14 different minimum energy structures. Overbars indicate the range of cluster volume plotted in Figure 5. Lines are merely intended to guide the eye.

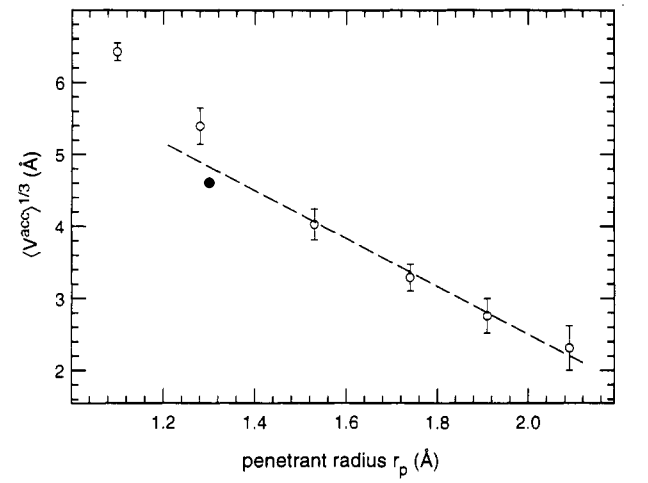

Figure 5. Cube root of the accessible volume corresponding to the peak indicated in each distribution of Figure 4, plotted as a function of penetrant radius. The error bars depict the uncertainty in the location of the peak in the distribution. The diamond is an experimental value from the o-positronium annihilation data of Lind et al.[47] (see text for details).

outward from the sorption states, as seen qualitatively in Figure 3 in the case of helium and smaller penetrants. Shown as a diamond in Figure 5 is an experimental value for the volume accessible to the center of o-Ps in quenched isotactic polypropylene at 233 K which we esimated from

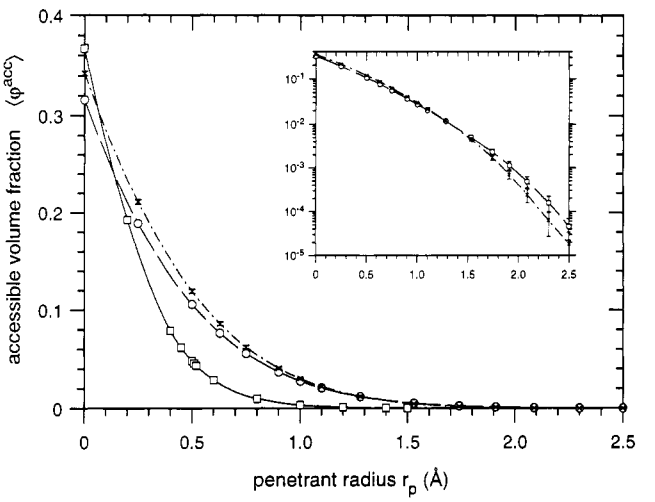

Figure 6. Accessible volume fraction $\langle\phi^{acc}\rangle$ as a function of penetrant radius r_p in rcp atomic glass (□), polymer glass (○), and polymer melt (×). The inset is a log plot of the polymer data. All lines are merely connections to guide the eye.

the positron annihilation work of Lind et al.[47] Only amorphous regions in the isotactic polymer were assumed accessible to o-Ps. The simple theory of Tao[46,48] was used to relate the reported lifetime of ca. 2 ns to an equivalent spherical hole radius of 2.9 Å, and hence an accessible volume of 98 Å^3. In displaying this experimental point in Figure 5, we have chosen to represent the positronium by a van der Waals radius of 1.3 Å, equal to that of the hydrogen atoms used in the polymer simulations. Although the polypropylene materials studied in the experiment and the simulation are not the same, agreement between the characteristic hole sizes seen in the experiment and the simulation is favorable. The simple theory relating hole size and o-Ps lifetime assumes spherical voids of equal size in the polymer; our calculations suggest a dispersity of shapes. Results from positronium lifetimes thus probably reflect the average over a variety of void shapes and sizes.

The average accessible volume fraction $\langle\phi^{acc}\rangle$ decreases with penetrant radius r_p, as shown in Figure 6. Physically, this expresses the simple fact that the center of a large penetrant can visit less of the unoccupied space than can the center of a small penetrant. The accessible volume fraction for a penetrant of zero radius is the average unoccupied volume fraction $\langle\phi^{unocc}\rangle$. Our value of $\langle\phi^{unocc}\rangle = 0.316$ compares favorably with 0.35 estimated from group contribution correlations in van Krevelen[49] and also compares well with the values of 0.354 and 0.31 calculated by Arizzi et al.[31] and Shah et al.,[30] respectively. The curves displayed in Figure 6 for the polymer melt and the random close-packed (rcp) atomic glass structure are discussed below.

Cluster Shape Results. The size and shape of clusters accessible to a particular penetrant are calculated from the radius of gyration matrix. Only nonpercolating clusters were subjected to this analysis, as only those have a finite radius of gyration. In the range $r_p > 1$ Å, the average root-mean-squared radius of gyration $\langle s^2\rangle^{1/2}$ of nonpercolating clusters decreases as the penetrant size increases, as shown in Figure 7. The dashed line depicts the result of a simple model calculation, wherein a spherical penetrant of radius r_p accesses monodisperse spherical holes of radius $R > r_p$. In this simple situation, the penetrant center would access a sphere with radius $(R - r_p)$; hence,

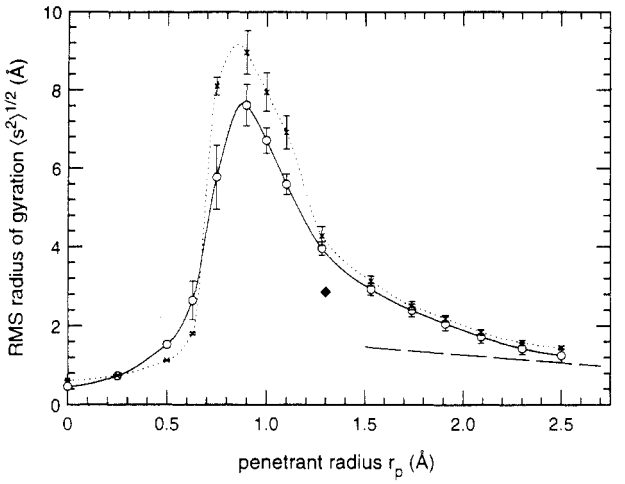

Figure 7. Root-mean-squared radius of gyration $\langle s^2 \rangle^{1/2}$ of nonpercolating clusters in the polymer glass (○) and the polymer melt (×) as a function of penetrant radius r_p. The dashed line represents a simple geometric model discussed in the text. The diamond shows the hole radius (not the radius of gyration) calculated from the positronium lifetime experiments of Lind et al.[47] Lines through the polymer data are only connections to guide the eye.

$\langle s^2 \rangle^{1/2}$ should be linearly related to r_p,

$$\langle s^2 \rangle^{1/2} = \left(\frac{2}{5}\right)^{1/2}(R - r_p) \tag{19}$$

from the expression for the moment of inertia of a sphere. This simple physical picture seems applicable as an asymptotic limit for the largest penetrants we investigated ($r_p > 2$ Å). The diamond in Figure 7 shows the equivalent sphere radius (not the radius of gyration) calculated from the o-Ps lifetime studies in isotactic polypropylene of Lind et al.[47] discussed above. Interpreting the experimental data requires an assumption of spherical voids. In this light, the qualitative agreement between simulation and experiment is satisfactory. The maximum in Figure 7 is a direct consequece of cluster percolation at small r_p. For a sufficiently small penetrant radius, few larger clusters remain unconnected to the infinite percolating cluster, as is qualitatively obvious from Figure 3 for radius 0.9 Å. In the limit of $r_p \to 0$, essentially all accessible volume lies in the infinite cluster.

The average asphericity of nonpercolating clusters, $\langle b/s^2 \rangle \approx 0.5$, was independent of penetrant radius within the error of the simulation. As a reference, asphericity equals 0 for a sphere, 1 for a line, and $^1/_2$ for an ellipsoid of revolution with principal axis lengths in the ratio 2:1:1.

Comparison of Polymer Melt and Glass. It is interesting to compare the geometric properties of the polymer glass with those of a polymer melt. The melt is less dense than the glass; the resulting increase in accessible volume is most apparent in Figure 6 for small radii. The accessible volume in the melt is practically indistinguishable from that in the glass for $r_p > 1.0$ Å. Figure 7 shows that the root-mean-squared radius of gyration of nonpercolating clusters in the melt equals that in the glass for helium and larger penetrants but exceeds that in the glass in the range 0.65 Å $< r_p <$ 1.3 Å. In this range of penetrant radii, accessible clusters contain many "fingers" emanating from large voids, as seen in Figure 3. An increase in $\langle s^2 \rangle^{1/2}$ suggests an increase in the spatial extent of these "fingers," implying that the larger unoccupied volume in the melt mainly augments the size of passages between sorption macrostates, rather than increasing the size of macrostates themselves.

Figure 8 illustrates the most significant difference between the accessible volume distributions in the glass and in the melt. Shown on the left for each temperature is the accessible volume distribution in particular configurations visited during the simulation. Shown on the right are the structures after 10^7 attempted NPTMC moves at 233 K (glass) and at 400 K (melt). In the glass, the clusters retain their identity, whereas in the melt the distribution of accessible volume is transitory. At sufficiently high temperatures, a penetrant will be carried along by fluctuations that drastically redistribute unoccupied space in the melt.[20] In the glass or low-temperature melt, on the other hand, the distribution of available volume is more or less permanent. Diffusion will most likely occur through infrequent jumps between clusters that are frozen in space.

Comparison of Polymer Glass with an rcp Atomic Glass. The geometric properties of our polymer system may also be compared with those of other amorphous materials. Shown in Figure 6 is a plot of accessible volume in a random close-packed (rcp) model of an atomic glass. This rcp system consists of a set of spheres interacting with one another via a Lennard–Jones potential and residing in a local minimum of the potential energy. The atomic coordinates for this system were generously supplied by S. L. Chan.[50] The calculated structure factor indicates the absence of crystallinity. The van der Waals radius of spheres in the rcp structure is 2 Å, which is commensurate with that of methylene, methine, and methyl segments in the polypropylene model. The atomic "granularity" of the rcp and polymer structures is thus comparable. Although the rcp structure has more unoccupied volume, the voids of the polymer can be occupied by much larger penetrants than the voids of the rcp structure. In other words, the average accessible volume fraction is larger in the polymer than in the rcp atomic glass for all non-zero radius penetrants studied.

Thermal Fluctuations in the Distribution of Accessible Volume. In addition to comparing structures separated by millions of attempted NPTMC moves, it is instructive to consider fluctuations in connectivity of the unoccupied space which occur as the glassy polymer simulation proceeds. Figure 9 displays the volume accessible to helium in four snapshots from one glassy simulation; 2×10^5 attempted moves separate successive snapshots. Snapshot a shows the initial isolated clusters. As the polymer fluctuates, a channel appears connecting two images of the yellow cluster (b). Also, the purple cluster disconnects from the back of the yellow cluster. As the simulation proceeds, the percolating yellow pathway begins to disappear (c) and ultimately vanishes (d). This type of channel opening has been observed in an MD simulation of oxygen diffusion in glassy polyethylene;[22] there the fluctuation lasted 10 ps. Here we see such a fluctuation even in the absence of a penetrant molecule.

Connectivity Results. The distributions $p(n)$ of the number of paths emanating from clusters accessible to argon and helium in the glass are shown in Figure 10. Clusters accessible to helium are very well connected. There are usually 12–20 clusters accessible to helium in each polymer configuration; the majority of clusters have paths leading to 3–4 other clusters. Some clusters are connected extensively, with paths leading to over 10 other clusters. In the case of argon, 2–6 clusters are typically accessible in each configuration; a plurality of clusters accessible to argon are connected to 2 other clusters.

Some clusters accessible to argon or helium are relatively isolated. For example, a cluster with one pathway

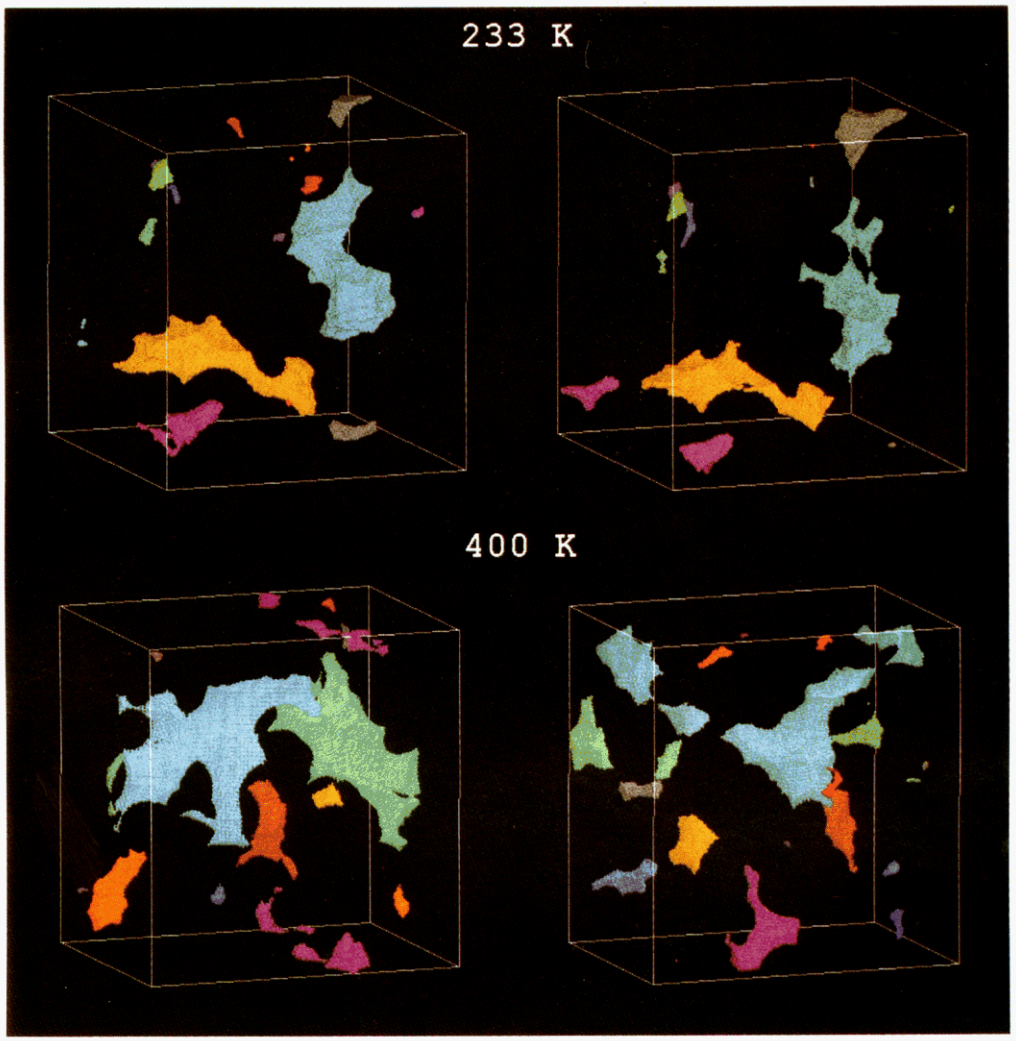

Figure 8. Clusters accessible to helium (r_p = 1.28 Å) in a polymer glass (233 K) and melt (400 K). 10^7 NPTMC moves were attempted between the structures on the left and on the right. Significant cluster reorganization occurs in the melt, whereas clusters are "frozen" in the glass.

emanating from it is an accessible "cul-de-sac". Clusters appearing connected to 0 or 1 other clusters are not totally isolated, however. Because we impose a lower limit on the probe radii used in the connectivity identification process, we close pathways that are accessible only to smaller penetrants. Extensive rearrangement of the polymer chains would be required to create a path which visits these clusters, implying that they are of less relevance in considering diffusion.

Percolation Properties. The connectivity of accessible volume determines the continuum percolation properties of the penetrant/glassy polymer system. In the limit of a zero radius penetrant, the unoccupied volume constitutes an infinite cluster of average volume $\langle\phi^{\text{unocc}}\rangle V$, where $\langle\phi^{\text{unocc}}\rangle$ = 0.316, the unoccupied volume fraction of the pure polymer, and V is the box volume. As larger penetrants are considered, connections in the infinite cluster close, until the percolating pathway spanning the system disappears, leaving a set of finite clusters. We refer to the critical radius at which the last pathway closes as the critical radius for percolation r_{p_c}. For an infinite size model system, r_{p_c} converges to a specific value. For the small model systems we use, one expects r_{p_c} to vary from configuration to configuration and to be subject to system size effects.

In order to quantify the onset of percolation, we invoke the tetrahedral tessellation of the polymer. Starting with small r_p, for which the system percolates, we plot in Figure 11 the average unoccupied volume fraction $\langle\phi_\infty^{\text{unocc}}\rangle$ of tetrahedra connected to the infinite path. If a tetrahedron belongs to the infinite path, we assign its full unoccupied volume (not its accessible volume) to the plotted average; tetrahedra not belonging to the infinite path do not contribute to the plotted average. Note that $\langle\phi_\infty^{\text{unocc}}\rangle$ does not diverge, although the absolute size of the infinite cluster does, since the size of the infinite cluster depends linearly on the size of the system. For small r_p, slight changes in penetrant radius have little effect on the tetrahedra comprising the infinite cluster; thus the unoccupied volume fraction does not change significantly. For the three 50-unit chain polymer systems examined here, the average percolation threshold occurs in the range 0.9 Å < r_p < 1.1 Å, for which the average unoccupied volume fraction of tetrahedra in the infinite cluster $\langle\phi_\infty^{\text{unocc}}\rangle$ tends to zero. For radii above this critical range, no infinite cluster exists and $\langle\phi_\infty^{\text{unocc}}\rangle$ equals zero by definition. Since we are averaging over many small systems, a smooth curvilinear tail appears in $\langle\phi_\infty^{\text{unocc}}\rangle$ around r_{p_c}. A similar tail was observed by Takeuchi in his study of various hypothetical polymers.[51] Larger penetrants may percolate a small number of configurations, but this is due to the small size of these configurations. To investigate the effect of system size on the estimated percolation threshold, we prepared

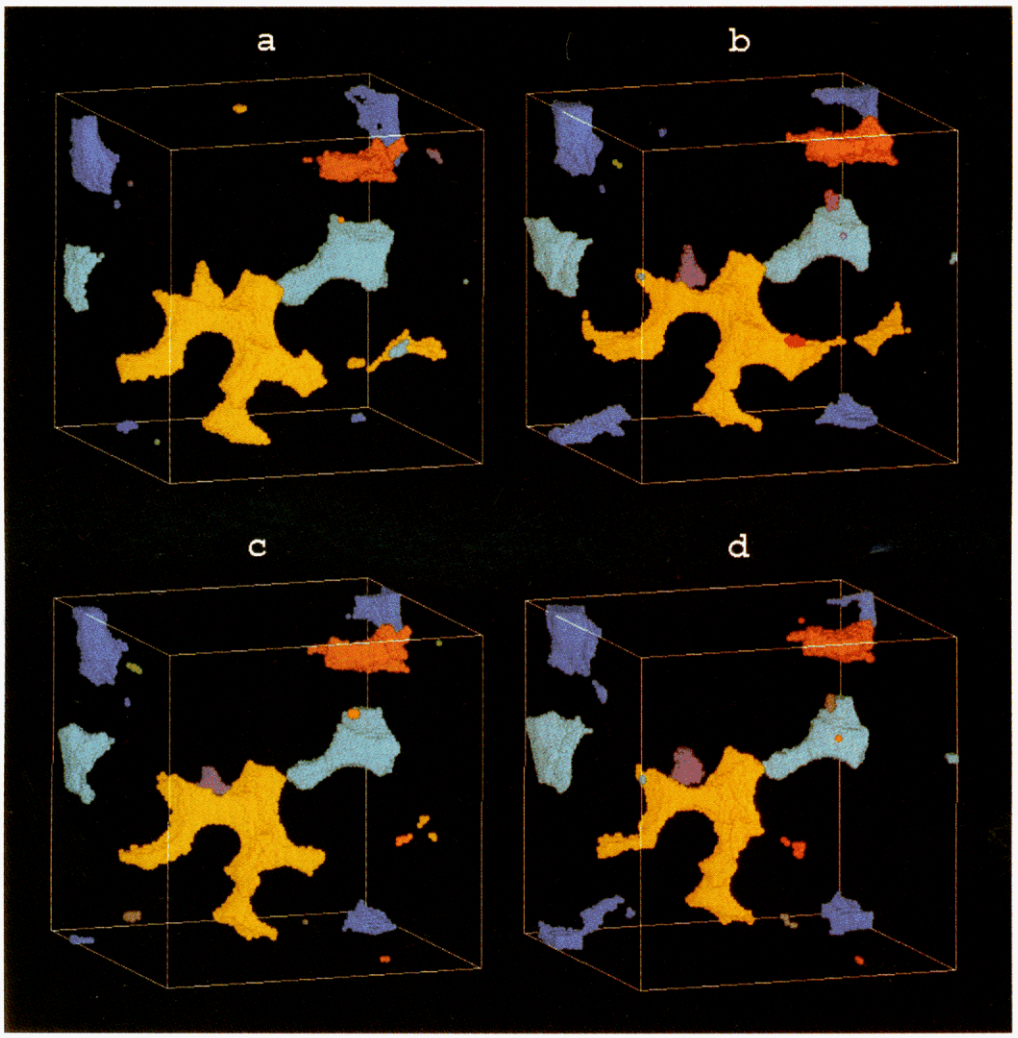

Figure 9. Clusters accessible to helium in four snapshots from an NPTMC simulation of pure polymer. 2×10^5 NPTMC moves were attempted between consecutive snapshots. In (b) a void opens between two images of the yellow cluster solely as a result of polymer fluctuations.

two systems containing two 50-unit chains each and one system containing six 50-unit chains. No distinguishable change was observed in the percolation behavior.

The percolation properties of the polymer and the rcp atomic glass structure are compared in Figure 11, and it is seen that percolation in the polymer appears for much larger penetrants than in the rcp structure. Clusters in the rcp structure are smaller and less polydisperse than in the polymer glass. The connectivity between atoms of the polymer tends to group the unoccupied volume into a few larger and many smaller clusters. As seen in Figure 9, few pathways through the polymer need to open to connect the larger clusters and enable percolation. The rcp structure, on the other hand, has a much less "patchy" unoccupied volume distribution, and many pathways must be opened in order to have the same effect. Unfortunately, the availability of only one rcp structure does not permit a very detailed analysis, as was performed in the glassy polymer case. Little curvature occurs in the rcp plot around r_{p_c} because only one structure was considered. Consideration of more rcp structures would spread the decrease in $\langle \phi_\infty^{\text{unocc}} \rangle$ over a somewhat broader range of penetrant radii. One can anticipate, however, that this finite size spread in the rcp results should not be as wide as that in the polymer, since rcp systems are intrinsically more homogeneous than polymer systems at these small length scales. The qualitative result that the onset of percolation occurs at much smaller radii in an rcp atomic glass than in glassy polymer structures of the same atomic granularity would thus remain valid.

The percolation threshold may also be defined in terms of the accessible volume fraction ϕ^{acc}. Previous work[52-54] investigated percolation of voids between overlapping, randomly located spheres (sometimes called a "Swiss-cheese" model). This void volume varies with the number density of spheres and corresponds to our accessible volume. The void volume fraction at the onset of percolation was found to be in the range 0.03 to 0.034 when spheres were placed randomly[52-53] or placed with a Bernal distribution.[54] From Figures 6 and 11, we estimate $\phi_c^{\text{acc}} = 0.035$ for the rcp atomic glass, in agreement with the corresponding result for the Swiss-cheese model. For the polymer, we estimate $\phi_c^{\text{acc}} = 0.02$–$0.04$, corresponding to the range $0.9 < r_p < 1.1$ Å in Figure 11. This is in agreement with the Swiss-cheese model and also compares favorably with Takeuchi's estimate of 0.055 for hypothetical polymers, within the error in his calculation of the accessible volume. These results suggest that the local spatial correlation present in the polymer and in the rcp atomic glass have only a small effect on the critical accessible volume fraction for percolation. The penetrant radius at which this critical value is achieved, however, is quite larger in the polymer than in the rcp atomic glass.

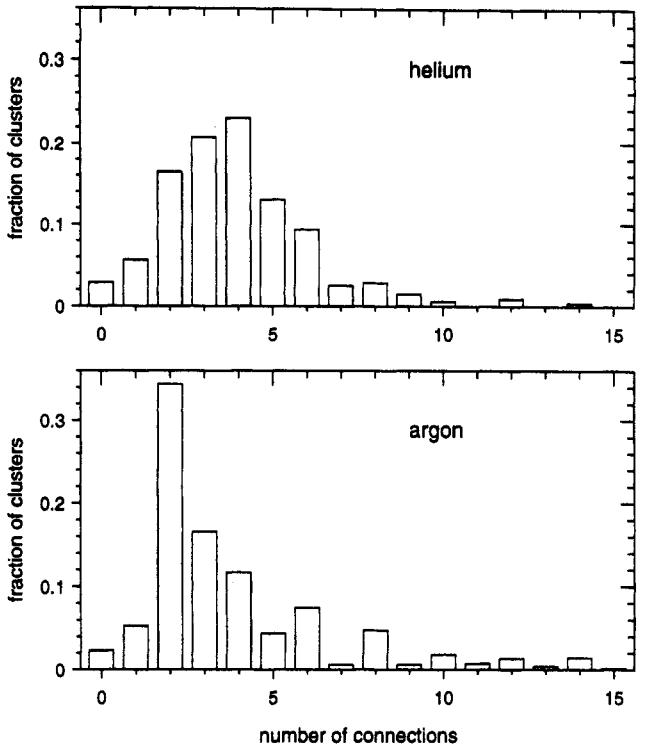

Figure 10. Distribution $p(n)$ of the number of pathways emanating from clusters accessible to (a) helium and (b) argon. Each such pathway leads to another cluster.

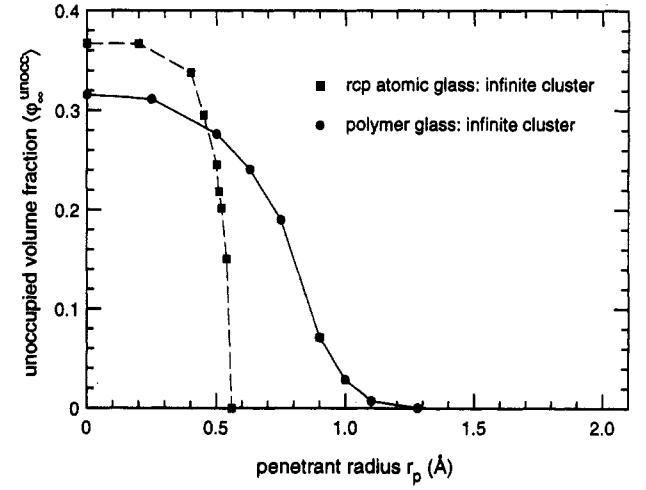

Figure 11. Unoccupied volume fraction of the infinite cluster $\langle \phi_\infty^{unocc} \rangle$ in rcp atomic glass (■) and polymer glass (●). A nonzero value signifies the onset of percolation.

Conclusions

Several conclusions can be drawn about the characteristics of clusters of volume accessible to penetrants in atactic polypropylene. A polydisperse distribution of sizes is found; i.e. not all clusters accessible to a particular penetrant are the same size. Although the probability of finding a particular cluster size generally decreases as a function of penetrant size, the decrease is not monotonic; some cluster sizes are more prevalent due to the local packing tendencies of polypropylene chains. The cluster sizes observed are commensurate with the sizes measured in positronium annihilation experiments on isotactic polypropylene.

Pathways accessible to hypothetical penetrants of small radius connect accessible clusters, and an algorithm has been described for quantifying the connectivity established by such pathways. It is found that 2–4 paths emanate from most clusters, depending on the penetrant radius. The accessible volume percolates for penetrants in the range $r_{p_c} \sim 0.9$–1.1 Å; this is significantly larger than the percolation threshold radius in a random close-packed system of spheres with roughly the same atomic radius as the segments of the polymer. The accessible volume percolation threshold is in the range $\phi_c^{acc} \sim 0.02$–0.04 for the polymer and $\phi_c^{acc} \approx 0.035$ for the random close-packed spheres; these compare favorably with the range $\phi_c^{acc} \sim 0.030$–0.034 observed previously for the percolation of void spaces between randomly placed spheres (a "Swiss-cheese" model).

The lifetime of clusters was found to depend on the state of the polymer. In a glass, no reorganization of clusters occurs after many Monte Carlo steps, whereas in the melt clusters undergo extensive rearrangement. Finally, it was shown that infrequent thermal fluctuations in the glassy polymer matrix may momentarily open a channel between two previously unconnected clusters. Such matrix fluctuations may play a significant role for the diffusive motion of sorbed penetrants. Multidimensional transition-state calculations in the penetrant and polymer degrees of freedom to quantify the average frequency, length, and mechanism of such hops are underway.

Acknowledgment. This material is based upon work supported under a National Science Foundation Graduate Fellowship to M.L.G. D.N.T. acknowledges financial support from the National Science Foundation PYI program (DMR - 8857659) as well as from Union Carbide, Inc. We also acknowledge NIH Grant 850RR05651A and T. Robinson for graphics support, T. D. Boone for the polymer structures, S. L. Chan for the rcp atomic structure, L. R. Dodd for the volume calculation program, E. M. Sevick for the connectivity algorithm, and the San Diego Supercomputer Center for a generous allocation of computer time.

References and Notes

(1) Vrentas, J.; Duda, J. *J. Polym. Sci., Polym. Phys. Ed.* **1977**, *15*, 403–416.
(2) Vrentas, J.; Duda, J. *J. Polym. Sci., Polym. Phys. Ed.* **1977**, *15*, 417–439.
(3) Vrentas, J.; Duda, J. *J. Polym. Sci., Polym. Phys. Ed.* **1977**, *15*, 441–453.
(4) Fujita, H. *Fortschr. Hochpolym.-Forsch.* **1961**, *3*, 1.
(5) Brandt, W. W. *J. Phys. Chem.* **1959**, *63*, 1080.
(6) DiBenedetto, A. T. *J. Polym. Sci.* **1963**, *A1*, 3477–3487.
(7) Pace, R.; Datyner, A. *J. Polym. Sci., Polym. Phys. Ed.* **1979**, *17*, 437–451.
(8) Pace, R.; Datyner, A. *J. Polym. Sci., Polymn. Phys. Ed.* **1979**, *17*, 453–464.
(9) Pace, R.; Datyner, A. *J. Polym. Sci., Polym. Phys. Ed.* **1979**, *17*, 465–476.
(10) Petropoulos, J. *J. Polym. Sci., Polym. Phys. Ed.* **1988**, *26*, 1009–1020.
(11) Jagodic, F.; Borstnik, B.; Azman, A. *Makromol. Chem.* **1973**, *173*, 221–231.
(12) Takeuchi, H.; Roe, R.; Mark, J. *J. Chem. Phys.* **1990**, *93*, 9042–9048.
(13) Müller-Plathe, F. *J. Chem. Phys.* **1991**, *94*, 3192–3199.
(14) Müller-Plathe, F. *J. Chem. Phys.* **1992**, *96*, 3200–3205.
(15) Müller-Plathe, F.; Rogers, S. C.; van Gunsteren, W. F. *Macromolecules* **1992**, *25*, 6722–6724.
(16) Boyd, R. H.; Pant, P. V. K. *Macromolecules* **1991**, *24*, 6325–6331.
(17) Trohalaki, S.; Rigby, D.; Kloczkowski, A.; Mark, J.; Roe, R. *Polym. Prepr. (Am. Chem. Soc., Div. Polym. Chem.)* **1989**, *30* (2), 23–24.
(18) Sonnenburg, J.; Gao, J.; Weiner, J. H. *Macromolecules* **1990**, *23*, 4653–4657.
(19) Pant, P. V. K.; Boyd, R. H. *Macromolecules* **1992**, *25*, 494–495.
(20) Pant, P. V. K.; Boyd, R. H. *Macromolecules* **1993**, *26*, 679–686.

(21) Sok, R.; Berendsen, H. J. C.; van Gunsteren, W. *J. Chem. Phys.* **1992**, *96*, 4699–4704.
(22) Takeuchi, H. *J. Chem. Phys.* **1990**, *93*, 2062–2067.
(23) Arizzi, S. Diffusion of Small Molecules in Polymeric Glasses: A Modelling Approach. Ph.D. Thesis, MIT, 1990.
(24) Gusev, A. A.; Arizzi, S.; Suter, U. W.; Moll, D. J. *J. Chem. Phys.* **1993**, *99*, 2221–2227.
(25) Gusev, A. A.; Suter, U. W. *J. Chem. Phys.* **1993**, *99*, 2228–2234.
(26) Takeuchi, H.; Okazaki, K. *J. Chem. Phys.* **1990**, *92*, 5643–5652.
(27) Theodorou, D. N.; Suter, U. W. *Macromolecules* **1985**, *18*, 1467–1478.
(28) Dodd, L. R.; Boone, T. D.; Theodorou, D. N. *Mol. Phys.* **1993**, *78*, 961–996.
(29) McKechnie, J. I.; Brown, D.; Clarke, J. H. R. *Macromolecules* **1992**, *25*, 1562–1567.
(30) Shah, V.; Stern, S.; Ludovice, P. *Macromolecules* **1989**, *22*, 4660.
(31) Arizzi, S.; Mott, P.; Suter, U. W. *J. Polym. Sci., Polym. Phys. Ed.* **1992**, *30*, 415–426.
(32) Trohalaki, S.; DeBolt, L.; Mark, J.; Frisch, H. *Macromolecules* **1990**, *23*, 813–816.
(33) Rigby, D., Roe, R. *Macromolecules* **1990**, *23*, 5312–5319.
(34) Weiss, G. H.; Bendler, J. T.; Shlesinger, M. F. *Macromolecules* **1992**, *25*, 990–992.
(35) Kirchheim, R. *Macromolecules* **1992**, *25*, 6952–6960.
(36) Gusev, A. A.; Suter, U. W. *Phys. Rev. A* **1991**, *43*, 6488–6494.
(37) Boone, T. D.; Theodorou, D. N. *Polym. Prepr. (Am. Chem. Soc., Div. Polym. Chem.)* **1992**, *33* (1), 513–514.
(38) Tanemura, M.; Ogawa, T.; Ogita, N. *J. Comput. Phys.* **1983**, *51*, 191.
(39) Allen, M.; Tildesley, D. *Computer Simulation of Liquids*; Oxford University Press: Oxford, U.K., 1987; p 21.
(40) Maitland, G. C.; Rigby, M.; Smith, E. B.; Wakeham, W. A. *Intermolecular Forces*; Oxford University Press: Oxford, U.K., 1981; p 508.
(41) Bird, R. B.; Stewart, W. E.; Lightfoot, E. N. *Transport Phenomena*; John Wiley & Sons: New York, 1960.
(42) Dodd, L. R.; Theodorou, D. N. *Mol. Phys.* **1991**, *72*, 1313–1345.
(43) Sevick, E. M.; Monson, P.; Ottino, J. *J. Chem. Phys.* **1988**, *88*, 1198–1206.
(44) Theodorou, D. N.; Suter, U. W. *Macromolecules* **1985**, *18*, 1206–1214.
(45) Zallen, R. *The Physics of Amorphous Solids*, 1st ed.; Wiley-Interscience: New York, 1983, Chapter 4.
(46) Deng, Q.; Jean, Y. *Macromolecules* **1993**, *26*, 30–34.
(47) Lind, J. H.; Jones, P. L.; Pearsall, G. W. *J. Polym. Sci., Polym. Chem. Ed.* **1986**, *24*, 3033–3047.
(48) Tao, S. J. *J. Chem. Phys.* **1972**, *56*, 5499–5510.
(49) van Krevelen, D.; Hoftyzer, P. *Properties of Polymers*; 2nd ed.; Elsevier: Amsterdam, 1976.
(50) Chan, S. L.; Elliott, S. R. *J. Non-Cryst. Solids* **1990**, *124*, 22–33.
(51) Takeuchi, H.; Okazaki, K. *Makromol. Chem., Macromol. Symp.* **1993**, *65*, 81–88.
(52) Kertész, J. *J. Phys. Lett.* **1981**, *42*, L393–L395.
(53) Elam, W.; Kerstein, A.; Rehr, J. *Phys. Rev. Lett.* **1984**, *52*, 1516–1519.
(54) Roberts, J. N.; Schwartz, L. M. *Phys. Rev. B* **1985**, *31*, 5990–5997.